7th ECCOMAS Thematic Conference on Smart Structures and Materials
SMART 2015
A.L. Araúo, C.A. Mota Soares, et al. (Editors)

EXPERIMENTAL INVESTIGATION OF A COMPLIANT MECHANISM FOR AN UAV LEADING EDGE

Martin Radestock*, Johannes Riemenschneider†, Hans-Peter Monner§, Michael Rose‡

German Aerospace Center (DLR)
Institute of Composite Structures and Adaptive Systems
Lilienthalplatz 7, 38108 Braunschweig, Germany
*E-mail: Martin.Radestock@dlr.de, † E-mail: Johannes.Riemenschneider@dlr.de
§ E-mail: Hans.Monner@dlr.de, ‡ E-mail: Michael.Rose@dlr.de

Keywords: Morphing leading edge, topology optimisation, morphing unmanned aerial vehicle, compliant mechanism.

Summary. *A description of a framework for a morphing leading edge will be given. The considered aircraft is an unmanned aerial vehicle with a span of 4 m. The first step of the framework is a skin optimisation with the main objective to realise a skin layup and a load introduction point in order to match given aerodynamic shapes. The second step is a topology optimisation to realise a kinematic inside the leading edge with a compliant mechanism. Due to ideal boundary conditions the simulation results have to be post processed for manufacturing. The experimental investigation will clarify the divergence between the simulation and the manufactured kinematic. The main objective of the experiments will be the deformation and the strain in the mechanism.*

1. INTRODUCTION

In order to improve the efficiency of aircraft a lot of mechanism were tested several years ago and are summed up in paper from Barbarino et al.[1] and Vasista et al.[2]. Many mechanism were collected in the paper to deform the wing like sweep, twist, oblique wings, etc. Next to such morphing wings a focus is set to the size of the airplane for special missions. Small aircraft are used to observe the climate and collect visual information. These tasks can be done without any human on board and therefore unmanned aerial vehicle (UAV) become nowadays more interesting. Even these aircraft can be improved with morphing mechanisms and they are investigated by Friswell and Inman [3] or Santos et al. [4]. In the context of the EU project CHANGE a combination of different morphing mechanisms is utilised for an UAV to extend the endurance of the aircraft. The morphing concepts are shown in Fig. 1. The flight missions define the required shapes of the wing and a selection of mechanisms for twist, camber and span extension is done. The baseline is an UAV with the span of 4m and a maximum takeoff weight of 25 kg. The baseline fuselage is provided by a model from TEKEVER and morphing wings are developed. The observation is the most time spending flight state and therefore this

will be the basis wing, which is a NACA 6510 profile. The morphing will be realised with a span extension and an independent leading edge and trailing edge camber variation, which can also provide a kind of twist. This paper will describe the realisation of the mechanism in the leading edge and the investigation of the deformation. The profile has a chord length of 60 cm and the leading edge morphing shall be implemented in 30 % of the chord. The challenge here is the separation of each mechanism in their design space. Therefore the actuation, mechanisms and interfaces will be in the leading edge. Only the energy supply is deposited in the fuselage.

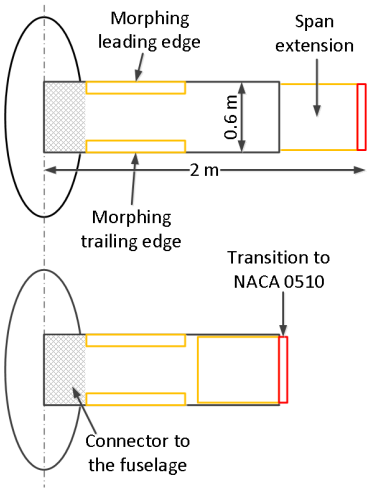

Figure 1. Morphing wing concept in CHANGE

The first part will describe the steps of the framework. This includes an optimisation of the skin which realises a layup and load introduction in order to reach the aerodynamic shapes. The second step of the framework is a topology optimisation to get a compliant mechanism which realises the deformation. Certain modelling characteristics like the idealized boundary conditions have to be changed for a proper manufacturing of the simulation results. The interfaces between the mechanism, skin and spar will be designed manually in a post processing step. The second part of the paper will describe the experimental investigation of the realised mechanism. Due to the post processing the divergence between the simulation model and the manufactured model will be investigated. The focus lays on the deformation of the mechanism and the strains in the material. This investigation will validate the framework and will be the starting position for the assembly of the leading edge module in CHANGE.

2. FRAMEWORK FOR THE LEADING EDGE

The overall process of the framework is shown in figure 2. Here are the different steps of the optimisations shown, starting by an aerodynamic shape and ending with manufacturing of the skin and the mechanism.

The three input profiles are the NACA 6510, 2510 and 3510. The maximum deformation is between the NACA 6510 and 2510 and the 3510 is seen as an intermediate state in the

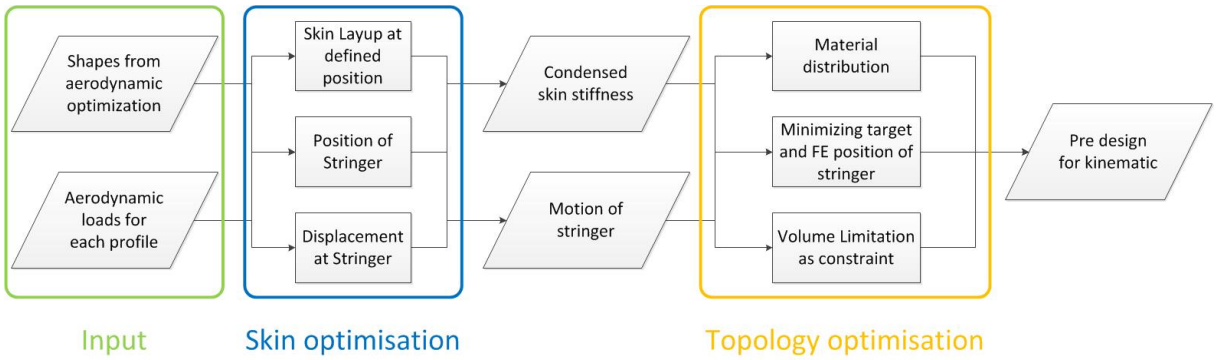

Figure 2. Process Chain of the framework

morphing. Based on the given aerodynamic shapes, the skin optimisation provides a skin layup distribution with glasfiber reinforced prepreg (GFRP) and ethylene propylene diene monomer (EPDM) rubber, a stringer position as a load interface point for the inner mechanism and the motion path of the stringer due to deformation. The topology optimisation as second step will give a pre design of an inner kinematic which will be manufactured as compliant mechanism.

2.1 Skin optimisation

Figure 3 shows the different shapes which are necessary for the optimisation and the position of the front spar, which is set by 30 % of the chord length. The perimeters P of the given NACA profiles, which are properly scaled to be connected to the same spar, are slightly different. The NACA 2510 has a shorter perimeter than the NACA 6510 and therefore the longer profile is adapted to the same perimeter length. Otherwise it is not feasible to morph from one NACA profile to another one. The adjustment is done by a translation of the NACA 6510 to positive x direction. This was achieved in an iterative scheme until the sum of the distances between nearby points of each profile became equal. The translation is done until both sums of the NACA profiles are equal.

The skin optimisation based on the work of Kintscher et. al[5] and Monner et. al[6] for a smart droop nose. The initial shape is selected by the longest mission phase, which will be a loiter status with low speed conditions. The NACA 6510 is set as this starting profile. In case of the small dimensions and the deformation from round about 12 mm between the top of the NACA 2510 and 6510 the skin will have a uniform layup. The stacking is 0.5 mm of EPDM as top and bottom layer and three GFRP layers with 90° /0° /90°, where 0° is equal to the chord wise direction. The stringer number will be limited in case that one load introduction point is sufficient to morph from one shape to another one. Especially the curvature of the shape will not change so much by such small deformations. The results will visualise this fact later on. The underlying SIMPLEX optimisation has only the position of one omega stringer and the deflection at the stringer as variable parameters. The finite element calculation within the optimisation considers the aerodynamic loads of the wing and determines the stringer position and deflection under these loads. The details of the skin optimisation are given in the PhD thesis

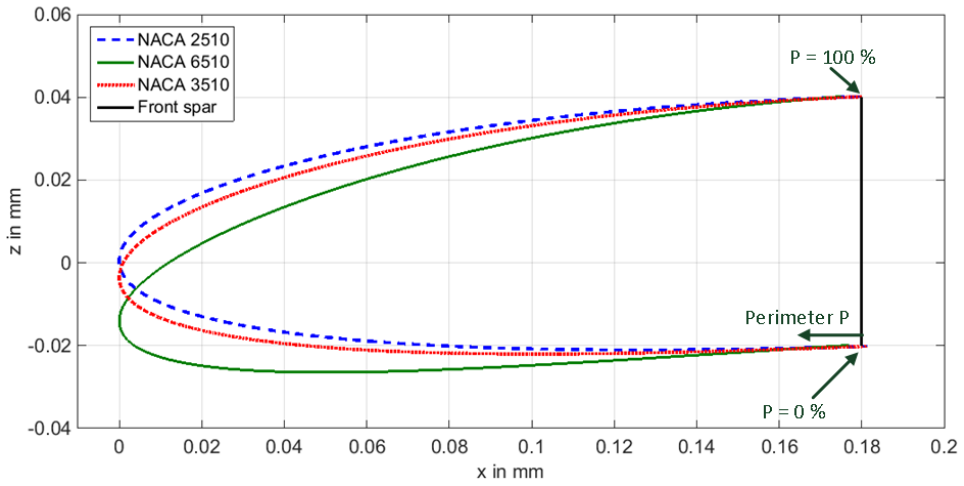

Figure 3. Leading edge geometry

of Kintscher [7] for a similar problem.

2.2 Topology optimisation

The skin optimisation delivers a certain stringer position, the deflection and the skin layup. These parameters will be used for the subsequent topology optimisation. At first the NACA 6510 profile is embedded in a regular grid structure. The optimiser can distrubute material in each grid cell using values between zero (whit, void) or one (black, full). In order to obtain a feasible structure, only the elements inside the leading edge are used like the dark grey elements in Fig. 4.

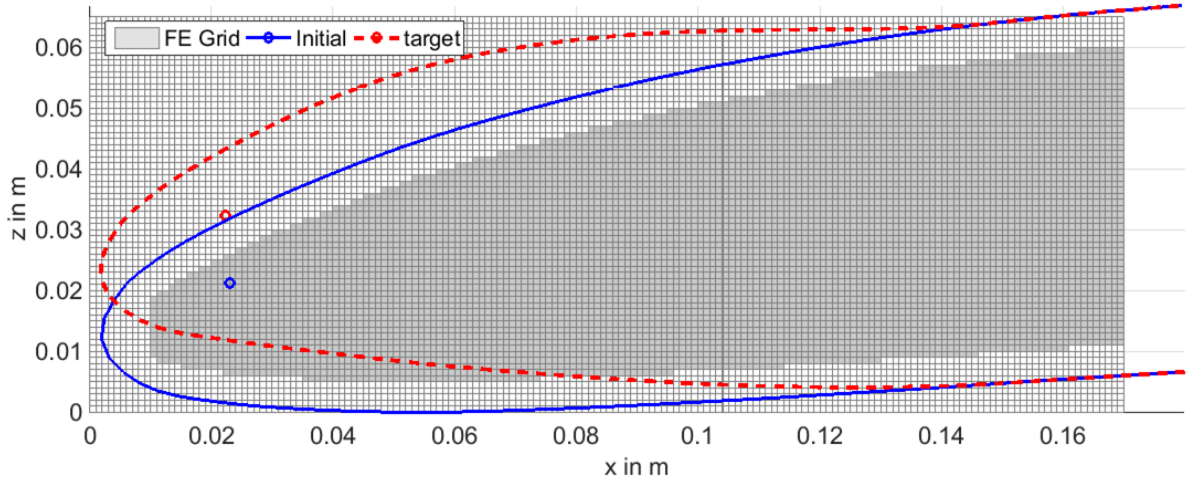

Figure 4. Initial design of topology optimisation

The boundary conditions for the optimisation are shown as well in Fig. 4 with a solid bearing at the right edge of the design room and a force F below. In case of the upward motion of the stringer from NACA 6510 to 2510, the force is set near the bottom part of the skin in order to obtain a supported moving direction. Another important aspect is the skin stiffness, which has to be included in the topology optimisation. Therefore the skin model is condensed to the stringer point in ANSYS ® and added to the stiffness matrix in the topology optimisation.

The algorithm of the topology optimisation follows a scheme, which is equal to the solid isotropic material with penalisation (SIMP) and described in Bendsøe and Sigmund [8]. The scheme contains at first an initial guess of the design space which is shown in Fig. 4 in dark grey. Afterwards a finite element calculation is done in order to get the acutal position of the stringer when the boundary conditions are present. The next step is the calculation of the main objective function, a sensitivity of the variables and a volume constraint. Than a gradient based optimiser called method of moving asymptotes (MMA) utilised the main objective function, the sensitivity and the volume constraint to obtain a new material distribution [10], [11]. Now a loop is starting with the next finite element calculation. This loop and the mathematical formulation is implemented from the work of Pedersen [9] and was adjusted to the case of the leading edge.

The main objective function minimizes the quadratic divergence between the target position of the stringer, which is the red circle in Fig. 4, and the actual position after the finite element calculation of the mechanism. The actual position depends on the material distribution, the blue circle in Fig. 3 indicates the position for the undeformed leading edge.

The volume constraint is selected with a maximu fill of 30 % of the active design space. It is an important side condition for the topology optimisation to make solution with too much material infeasible. A short summary of the topology optimisation can be done with the following equations.

$$min_{\ \xi}\ \ (||u_{act} - u_{tar}||_2) \tag{1}$$

$$s.t.: \qquad \frac{V^*}{V_{max}} - 1 \leq 0 \tag{2}$$

$$0 < \xi \leq 1 \tag{3}$$

where ξ is the design variable, u_{act} defines the vector with the actual position out of the finite element calculation, u_{tar} is the target position vector of the stringer, V^* is the actual filling of the design space and V_{max} defines the maximal filling of the design space.

The result is a pre designed structure where the elements of the grid will have nearly a full or void filling. Due to the continuous material distribution as a result from the topology optimisation, the volume constrained might only be achieved approximately. This will be accepted and has no major impact on the manufactured mechanism.

2.3 Simulation results

The framework delivers different structural results which will be summarised in this part. The first set was the layup of the skin with three layers of GFRP (90°/0°/90°) and 0.5 mm EPDM at the top and bottom of the GFRP layers. The uniform stacking will lead to a noticeable difference between the target shape and the optimised shape and can be seen in Fig 5 (a). If there was a stacking also done in the optimisation than the FE model would match the target shape better, but the stiffness of the skin will increase so hard that the required actuation force at the stringer will increase as well. Therefore this simple uniform skin was used and the divergence will be accepted for the morphing mechanism. Another point in Fig 5 (a) is the boundary condition of the FE model. The model has a solid bearing between 0.15 m and 0.18 m in x direction on the upper and lower skin in order to regard the connection to a C-spar. Therefore the optimiser is not able to match the NACA 2510 exactly. The omega stringer position is at 55.4 % in the perimeter direction, which is near to the top of the leading edge at the upper surface. To obtain the deformation result in Fig 5 (a) the deflection of 11.1 mm is necessary in z direction at the stringer.

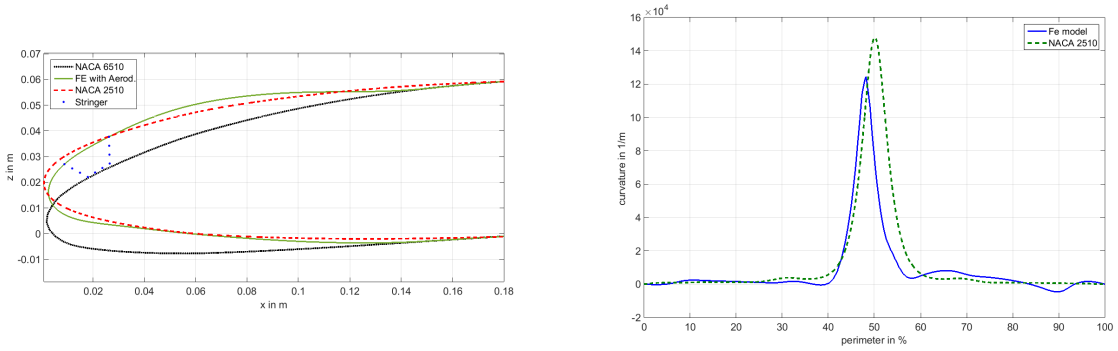

(a) Shape comparison of skin optimisation (b) Curvature of NACA 2510 and skin optimised model

Figure 5. Results of the skin optimisation

Another result out of the skin optimisation can give an estimation of the real skin to aerodynamic flow. Therefore the curvature of the structure is shown in Fig. 5 (b). A critical position along the perimeter is at 90 %, because the curvature changes the sign and this results in a bump of the skin. It cannot be seen directly in Fig 5 (a), but the critical position is on the upper side near to the C-spar and can be poorly influenced with the stringer and the deflection. Thus will be accepted and the influence at this position will be evaluated in a following wind tunnel test.

The design of a possible kinematic is shown in Fig. 6 as a result of the topology optimisation. It is possible to identify certain structure parts and the associated task. The red parts show a rigid structure of rods while the green part is a flexible hinge for the up and down motion. The rod where the actuation force F is initiated will not have any flexible component and conduce in common to transfer the force.

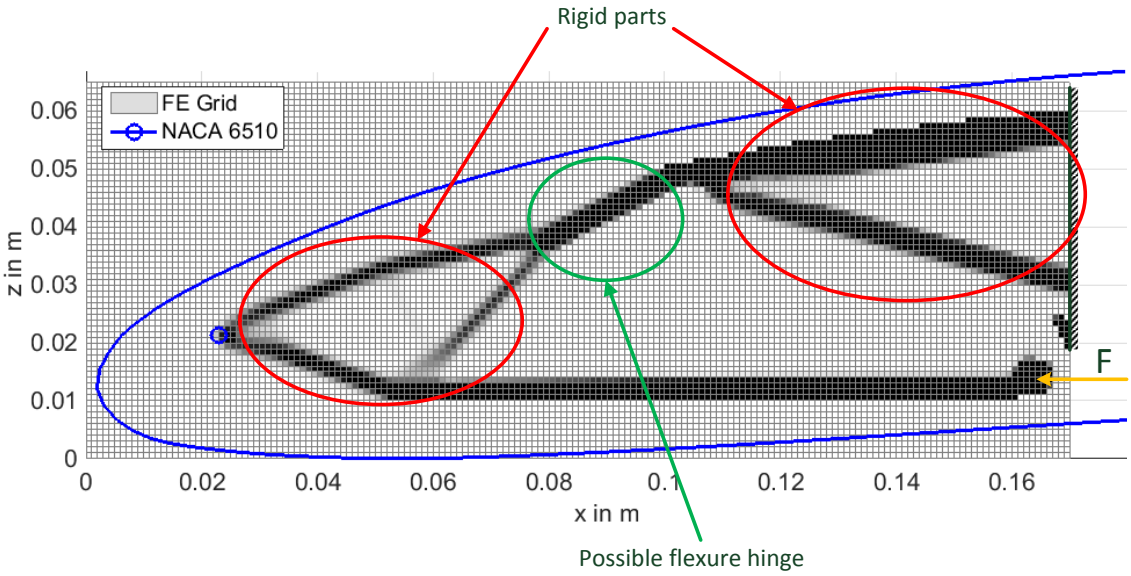

Figure 6. Result of the topology optimisation

2.4 Postprocessing and manufacturing

With the design idea of the topology optimisation a mechanism can be designed and realised with an additive manufacturing process. The procedure is the fused deposition modeling with a thermoplastic polyactide acid (PLA). Several problems raise through a final design process, which can be seen in the difference between Fig. 6 and 7. The basic idea with rigid parts and the flexure hinge is maintained, but mostly the perfect boundary conditions in the topology optimisation have to be adapted for the real structure. One significant modification is the overall size of the compliant mechanism. The C-spar and the connection interfaces have to end at 0.18 m chord length, because the wing-box is connected right behind the spar. In the topology optimisation were only 2 cm provided for the spar and the interfaces, which was not feasible. Therefore the mechanism was scaled down to 0.13 m in chord wise length.

The actuation force was simulated as transversal force along the x axis, but the realisation will be done with a servo actuator. This will support the upwards motion of the stringer, because of the rotation around the flexure hinge, but it will change the motion at the stringer position as well. Another modelling aspect results of the flexure hinge. In the topology optimisation in the green region of Fig. 6 is a massive rod. The function as hinge will be full filled, but a lot of actuation energy is needed to deform the hinge. Most of the actuation force will be used for the elastic deformation instead of deforming the skin. The problem is that the topology optimisation tries to reach the target position and does not regard any stress in the mechanism. In order to reduce the actuation force a design with arcs was used, which distributes the stress along the flexure hinge. The design advices from literature were used here[12].

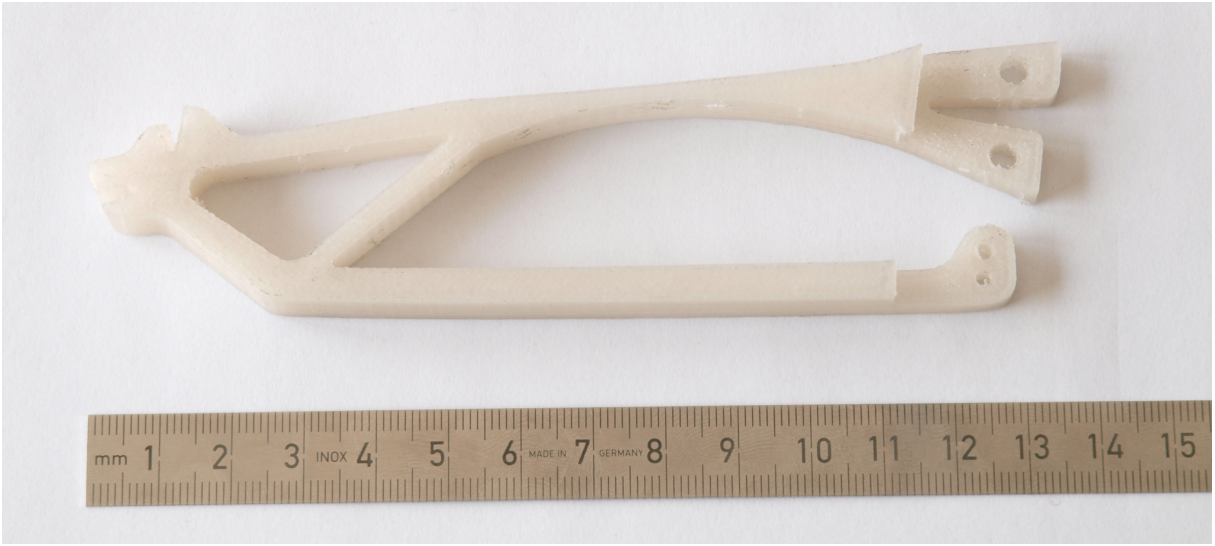

Figure 7. Manufactured compliant mechanism

After the modelling process the mechanism was simulated in ANSYS® without loads resulting by the skin. Here an input displacement at the actuator connection is utilised with 7 mm in negative x-direction. The results of the displacement in meter and the strain can be found in Fig. 8. The maximum occurring strain is expected in the flexure hinge with 1%. Simultaneously the maximum displacement in z-direction is 18.7 mm and is located at the stringer connection.

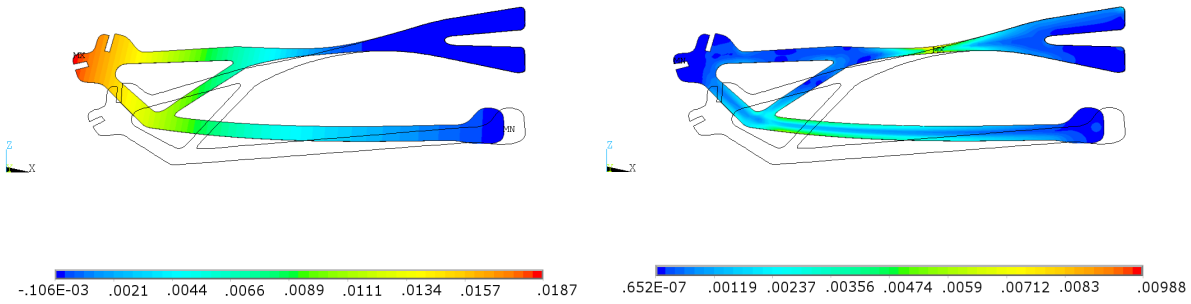

(a) Simulated displacement (b) simulated vonMises strain

Figure 8. Simulated results from ANSYS®

3. EXPERIMENTAL INVESTIGATIONS

All these changes and modelling aspects, which are not regarded in the optimisation process, have effects to the overall deformation. Therefore it is necessary to investigate the influence of the changes to the kinematic. This part will describe the experimental set up to investigate the deformation and the strain of the compliant mechanism and the expected skin deformation.

3.1 Experimental setup

The measurements are done in two ways to obtain the deformation and the strain in the kinematic. Both experiments are done with optical measurement in order to prevent e.g additional stiffness at the flexure hinge. The first experiment will show the deflection behaviour at the stringer interface of the kinematic in the regarded range. The second experiment will investigate the maximum deflection of the kinematic at the upper contour and analyses the strain in the maximal and minimal position.

The considered range is given by the control of the actuator and determined to this position. In order to reach the 11.1 mm from the skin optimisation the actuator has to drive 25 to 30 degree. Therefore the maximum position is set to ϕ = 30 degree at the actuator. The minimum position cannot be set out of aerodynamic shapes or requirements from the framework. Thus the minimal position is set to ϕ = -20 degree so that the kinematic does not get strained to high.

The solid bearing and the connection to the actuator is similar in both experiments. The first experiment is shown in Fig. 9 and contains a laser displacement measurement system. The overall range of the sensor provides 100 mm and is gathered with an oscilloscope. The upper limit of 50 mm will be shown as 10 V. A plate is attached to the mechanism to provide a horizontal plain. It cannot be excluded that the plain will not be horizontal while the compliant mechanism is moving, because the flexure hinge bends and upward motion of the mechanism is combined with a rotation at this hinge.

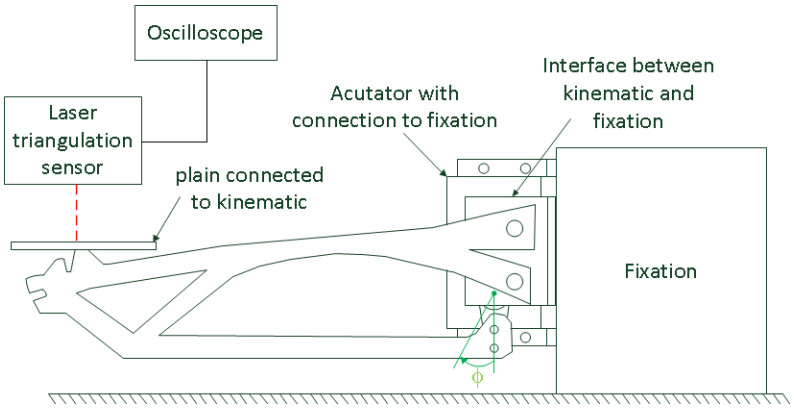

Figure 9. Setup of the first experiment

The second experiment is performed with the digital image correlation system ARAMIS from the GOM company. The schematic setup is shown in Fig. 10. Here are two cameras

disposed from the top view of the mechanism which gathers two different perspectives. The software is capable to measure the displacement of the contour from one position and can calculate the strain at the surface of the structure. Therefore a stochastic pattern is required at the surface. This pattern has to be high in contrast. The mechanism is manufactured out of a white thermoplastic and to provide a high contrast,a black colour is sprayed on. The ARAMIS will identify the stochastic pattern with the cameras and assign it to the different deformation conditions. This experiment will only regard the maximum and minimum position of the mechanism. In order to raise the load the mechanism will be driven to ϕ = 40 degree and ϕ = -30 degree.

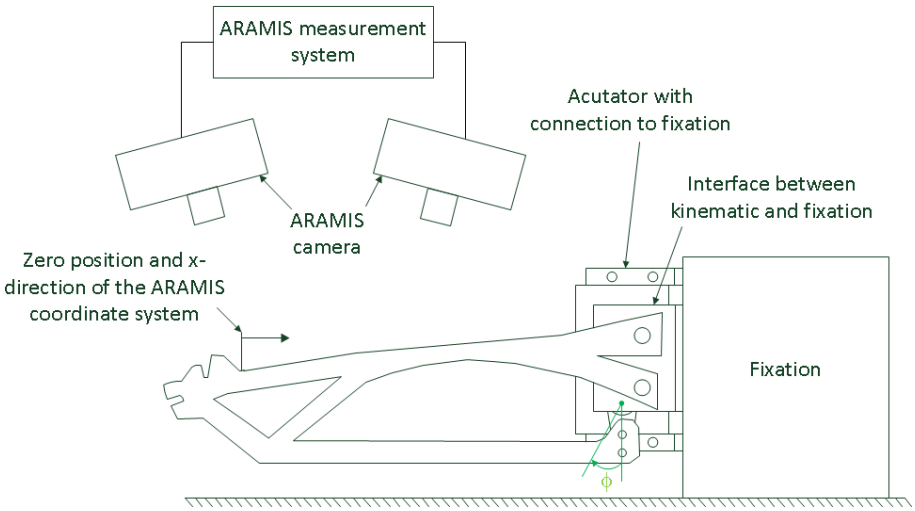

Figure 10. Setup of the second experiment

3.2 Experimental procedure

In the first experiment the deflection is observed while the actuator starts from zero degree up to 30 degree in steps of 5 degree. For each step, the voltage at the oscilloscope is documented. Afterwards the mechanism reversed to the starting position. Than the deformation is repeated for the upward motion 10 times and the values will be averaged. As second part, the downwards motion to -20 degree is done in steps of 5 degree. Here the displacement are recorded as well and the procedure is repeated 10 times. The repetition shall only prevent large derivation in the deflection.

The second experiment starts with the calibration of the ARAMIS measurement system. Than the mechanism is measured two times at the starting position in order to calculate the divergence in deflection and strain from the system. The difference between the first and second data set gives an estimation of the error of the system. The next step is to proceed the mechanism up to 40 degrees and gather the data. The next measured set is the zero degree position in order to observe elastic or plastic deformation at the mechanism. Than the procedure is repeated with control of the actuator to -30 degree.

3.3 Experimental results

The first experiment deliver the voltage from the oscilloscope which was transformed to a displacement. The displacement range of the laser sensor is 50 mm for the upper limit and -50 mm for the lower limit. The upper limit is equal to 10 V at the oscilloscope, -10 V for the lower limit and the values in between are linear interpolated. The Fig. 11 shows the transformed and averaged displacement of the 10 iterations for lift and droop control.

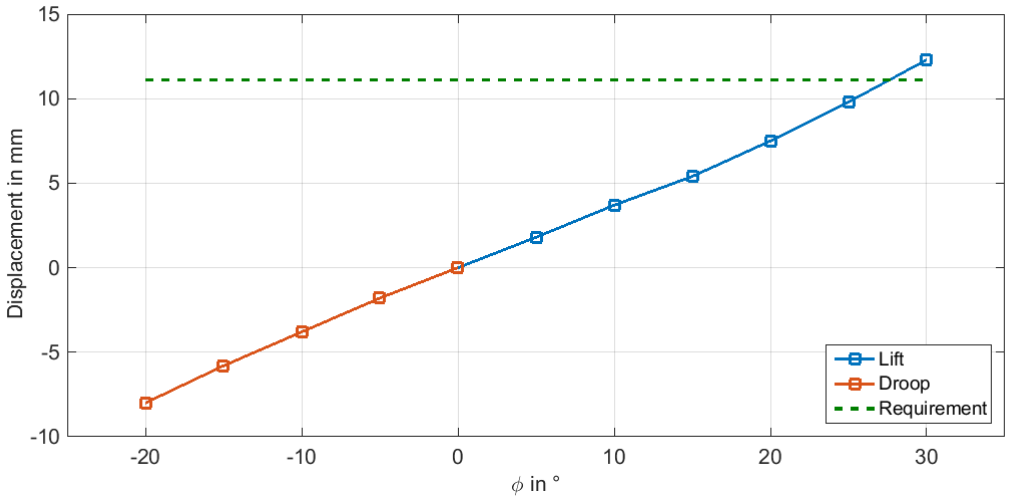

Figure 11. Results of the first experiment

The first experiment gives a first insight on the plastic deformation of the mechanism, too. In case of intensive plastic deformation a divergence in the 10 iterations between the zero position values can be recognized. The observed maximum divergence between the zero position values is 0.2 mm.

The second experiment observes the upper side of the kinematic and delivers the whole contour of the compliant mechanism. At first the mechanism remains in the zero position and two pictures were taken. Between these two are the displacement and strain calculated and shown in Fig. 12. This give an estimation of an error between the measurements. For the most part of the structure the displacement error is lower than 0.1 mm and the strain error lower than 0.15 %.

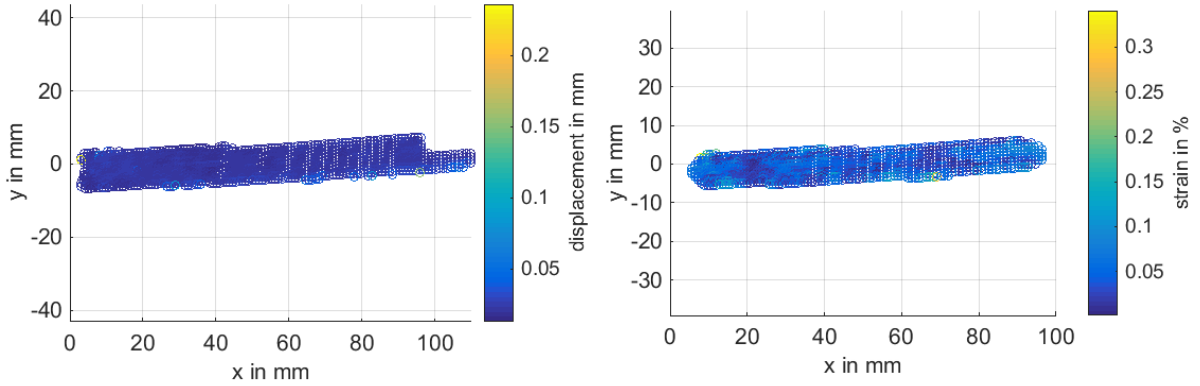

(a) Displacement error (b) vonMises error

Figure 12. Error of the measurement system

The results of the deformation and the vonMises strain in the lift position are shown in Fig. 13. It can be noticed that the maximum displacement is approximately at 14 mm while the maximum vonMises strain is 1.1 %. The maximum arises by 70 mm in x direction which is the position of the flexure hinge and can be compared with the manufactured mechanism in Fig. 7. It accomplishes the expectation, that mostly the hinge bends when compliant mechanism moves. The rest of the structure is quite stiff so that the strain is low with less than 0.3 %.

Fig. 13 confirms the simulation results from Fig. 8. The maximum vonMises strain and the displacement at the mechanism are similar and show the validation of the simulated compliant mechanism. Deviation exists, because the manufacturer of the PLA cannot provide any material properties and estimations were used [13]. Another aspect is the different actuation between the simulation and the experiment. In the experiment was a servo motor utilised while the simulation is done with a displacement. This could cause deviations, too.

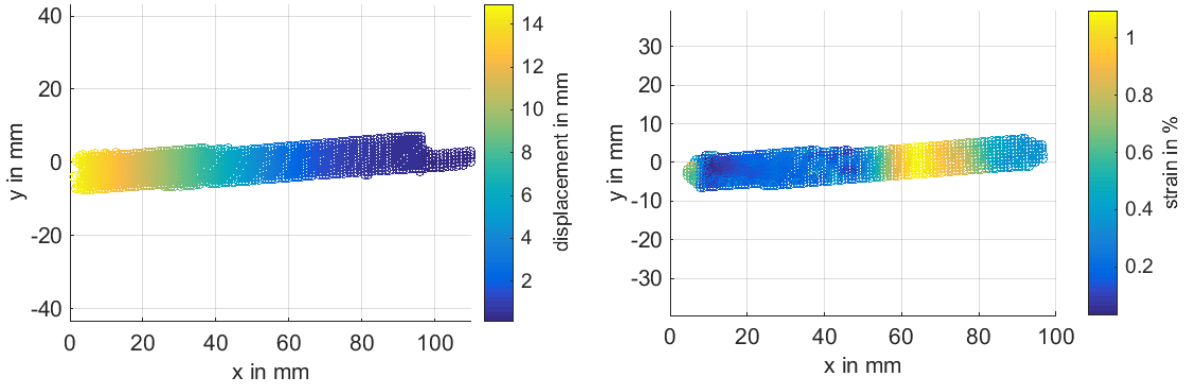

(a) Displacement (b) vonMises

Figure 13. Lifting the mechanism

The downward motion of the compliant mechanism shows similar results in displacement along the contour and the expected strain. The maximum displacement in Fig. 14 (a) is at about 10 mm and the maximum strain in Fig. 14 (b) approximately 1%. Here the bending is also in the flexure hinge where the strain peak rises. The rigid part are still stiff and therefore the motion between the flexure hinge and the stringer can be seen as a rigid body motion.

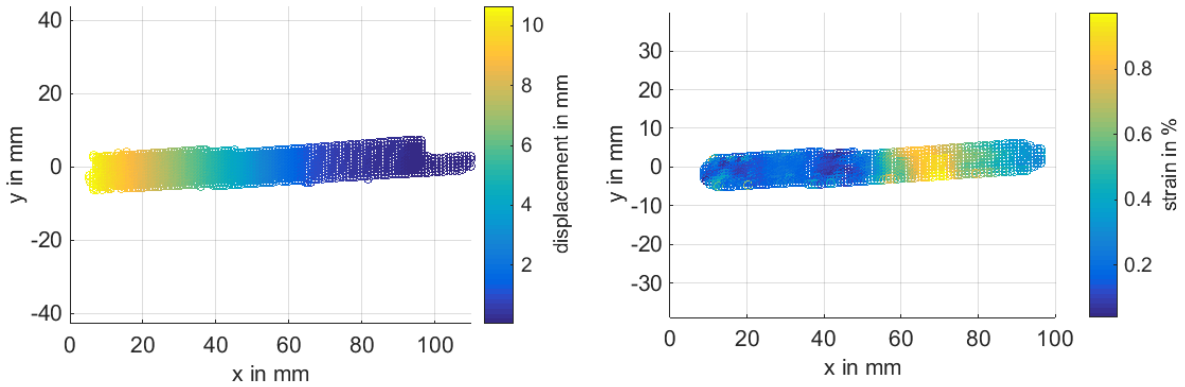

(a) Displacement (b) vonMises

Figure 14. Drooping the mechanism

From a material viewpoint the thermoplastic has a maximum strain of 1.1 % for the driven positions. Unfortunately there is no data-sheet available for this polyactide acid and the range of the parameter varies strongly. In case of different mixtures of the thermoplastic it is hard to find an estimation for any material properties and each manufacturer provides different data. Therefore an value for elongation at break was selected with 2.4 % of pure PLA, which is brittle

material in the pure form [13]. The elongation of break is higher than the measured data. So it is estimated that the material in the experiment is loaded in the elastic deformation range and can be provided as compliant mechanism for the leading edge.

4. CONCLUSION

The paper shows the process of a morphing leading for an UAV starting by aerodynamic shapes and the associated loads. There are several problems which raise between the framework and the utilised boundary conditions and the manufacturing process. For this leading edge a compliant mechanism can be provided with an topology optimisation and an additive manufacturing process. It is shown, that different post processing changes like modelling of flexure hinges or interfaces do not reduce the capability of the mechanism to reach the target deformation. Also the utilised material is suitable as compliant mechanism and can be applied for the morphing leading. The next step will be a wind tunnel test of the full scale model of the wing with this compliant mechanism. Then the shape accuracy can be evaluated with the framework.

References

[1] Silvestro Barbarino, Onur Bilgen, Rafic M. Ajaj, Michael I. Friswell and Daniel J. Inman, A Review of Morphing Aircraft. *Journal of Intelligent Material Systems and Structures* **22**, 823–877, 2011.

[2] Srinivas Vasista, Liyong Tong, and K. C. Wong, Realization of Morphing Wings: A Multidisciplinary Challenge. *Journal of Aircraft* **49**, 11–28, 2012.

[3] Michael I. Friswell and Daniel J. Inman, Morphing Concepts for UAVs. *21st Bristol UAV Systems Conference*, 13.1–13.8, April 2006.

[4] João R.C. Mestrinho, João M.I. Felício, Pedro D. Santos, Pedro V. Gamboa, Design Optimization of a Variable-Span Morphing Wing. *2nd International Conference on Engineering Optimization*, Lisbon, 6-9 September 2010.

[5] Markus Kintscher and Martin Wiedemann, Design of a Smart Leading Edge Device. *Adaptive, tolerant and efficient composite structures*, Springer-Verlag Berlin Heidelberg , 2013.

[6] H.P. Monner, M. Kintscher, T. Lorkowski, S. Storm, Design of a Smart Droop Nose as Leading Edge High Lift System for Transportation Aircrafts. *50th AIAA/ASME/ASCE/AHS/ASC Structures, Structural Dynamics, and Materials Conference*, Palm Springs, California, 4-7 May 2009.

[7] Markus Kintscher, *Entwurfsmethode für formvariable Flügelvorderkanten*. Forschungsbericht 2014-23, ISSN 1434-8454, Deutsches Zentrum für Luft- und Raumfahrt,2014 .

[8] Martin P. Bendsøe and Ole Sigmund, *Topology optimization. Theory, Methods and Applications*. Springer-Verlag Berlin Heidelberg , 2003.

[9] Claus B. W. Pedersen, Thomas Buhl and Ole Sigmund, Topology synthesis of large-displacement compliant mechanisms. *International Journal for Numerical Methods in Engineering* **50**, 2683–2705, 2001.

[10] Krister Svanberg, The method of moving asymptotes: A new method for structural optimization. *International Journal for Numerical Methods in Engineering* **24**, 359–373, 1987.

[11] Krister Svanberg, Some modelling aspects for the MATLAB implementation of MMA. *Internal publication of the KTH*. Devision Optimization and Systems Theory, September 2004.

[12] Nicolae Lobontiu, *Compliant Mechanisms: Design of Flexure Hinges*. CRC Press LLC London, New York, 2003.

[13] Aji P. Mathew, Kristiina Oksman and Mohini Sain, Mechanical Properties of Biodegradable Composites from Poly Lactic Acid (PLA) and Microcrystalline Cellulose (MCC). *Journal of Applied Polymer Science* **97**, 2014–2025, 2005.